Title

Adiabatic matching of particle bunches in a plasma-based accelerator in the presence of ion motion

Journal

Physics of Plasmas, 28(5)

ISSN

1070-664X

Authors

Benedetti, C
Mehrling, TJ
Schroeder, CB
et al.

Publication Date

2021-05-01

DOI

10.1063/5.0043847

Peer reviewed

Adiabatic matching of particle bunches in a plasma-based accelerator in the presence of ion motion

C. Benedetti,[1, a)] T.J. Mehrling,[1, b)] C.B. Schroeder,[1, 2] C.G.R. Geddes,[1] and E. Esarey[1]
[1)] *Lawrence Berkeley National Laboratory, Berkeley, California 94720, USA*
[2)] *Department of Nuclear Engineering, University of California, Berkeley, California 94720, USA*

(Dated: 8 April 2021)

Witness beam stability and preservation of its ultra-low emittance have been identified as critical challenges towards realizing a TeV-class, plasma-based linear collider. In fact, the witness bunch parameters required by a future TeV-class collider have been expected to trigger hosing instability and background ion-motion, leading to emittance degradation and, potentially, to bunch loss. Recently, it has been shown that ion motion suppresses the hosing instability, and proper longitudinal bunch shaping can eliminate the ion-motion-induced emittance growth. In this paper we propose and analyze a plasma-based method to generate the shaped bunches that enable emittance preservation in the presence of ion motion. The method is based on an adiabatic matching procedure, where a bunch with an initially untapered profile is injected in the plasma accelerator stage with an energy low enough that ion motion effects are initially small. As the bunch accelerates it is adiabatically compressed, ion motion is gradually triggered, and the bunch slowly but continuously readjusts itself in the ion-motion-perturbed wakefield acquiring the desired taper. The production of tapered witness bunch profiles that minimize energy spread and preserve emittance for collider-relevant parameters could enable the use of plasma-based accelerators for high-energy physics applications.

I. INTRODUCTION

With their extremely high accelerating gradients, plasma accelerators (PAs) offer the possibility to deliver high energy charged particle beams over distances orders of magnitude smaller than achievable with conventional accelerator technology. Hence, PAs have attracted considerable interest as possible drivers for future, high-energy, linear colliders (LCs)[1–5]. In a PA, a laser pulse or charged-particle beam propagating in a plasma drives (via the ponderomotive force in the case of the laser, or via the space-charge field in the case of the beam) an electron plasma wave (or wakefield)[6]. The plasma wave has a relativistic phase velocity, and the electromagnetic fields associated with it are suitable for accelerating and focusing a witness particle beam properly delayed with respect to the driver. PAs have demonstrated the acceleration of high-quality, quasi-monoenergetic electron and positron beams with accelerating gradients of up to 10s of GV/m, several orders of magnitude larger that that of conventional, radiofrequency-based accelerators, presently limited to about 100 MV/m due to material breakdown[7–11].

It is anticipated that a future high-energy LC will likely operate at a center of mass energy $\gtrsim 1$ TeV, and will require a peak luminosity $\gtrsim 10^{34}$ cm^{-2} s^{-1} [12,13]. Reaching this luminosity will imply using intense witness beams with $N_b \sim 10^{10}$ particles, and normalized emittance $\ll 1$ μm in order to ensure a sufficiently small bunch size at the interaction point. Furthermore, efficiency considerations require that the witness bunch extracts a significant fraction of energy from the wake, at the level of several tens of percent[2,14], hence the PA stages in a LC will operate in a strongly-beamloaded regime.

Stability of the witness beam and preservation of its ultra-low emittance during acceleration have been identified as critical challenges towards realizing a PA-based LC[15]. In fact, owing to the strong coupling between the witness bunch and the wake, any initial asymmetry in the bunch distribution (e.g., centroid misalignment or bunch tilt, etc.) is exponentially amplified (hosing instability[16,17]), leading to emittance growth and, ultimately, to transverse beam breakup and beam loss. Another source of emittance degradation for the witness bunch is background ion motion. Typically, for collider-relevant beam parameters (i.e., high energy, small emittance, and high charge) the bunch density exceeds the background ion density, and the space charge field associated with the matched witness bunch is so strong that it induces background ion motion on the time scale of the bunch duration itself. This results in a slice-dependent and nonlinear perturbation of the transverse wakefield within the bunch, and, hence, emittance growth for a linearly matched bunch[18–20].

Generally, hosing can be mitigated by inducing a head-to-tail variation of the particle betatron frequency along the bunch (detuning). This can be done either via the introduction of an energy chirp (e.g., Balakin-Novokhatski-Smirnov damping)[21], or by means of longitudinal variations in the strength of the accelerating and/or focusing wakefields[22,23]. For instance, for a witness bunch accelerating in a PA stage operating in the linear or quasi-linear regime, there is a naturally occurring variation of the transverse wakefield along the bunch that suppresses hosing[24]. On the other end, if the PA stage operates in the blowout regime, the strength of the transverse

[a)] Electronic mail: cbenedetti@lbl.gov
[b)] Now at Carl Zeiss SMT, Germany

wakefield is uniform along the witness bunch. Thus, a chirp of the betatron frequency could be induced by introducing a correlated energy spread along the particle beam. However, this option is not desirable for collider applications since for strongly-beamloaded stages the energy spread required to suppress the hosing instability is on the order of several percents[15,23], and this might render the transport and focusing of the bunch challenging. Recently, it has been shown that the slice-dependent wakefield perturbation due to the ion motion induced by a bunch with collider-relevant parameters can suppress hosing and allows for a stable witness bunch propagation in a strongly-beamloaded PA stage in the blowout regime[25]. Furthermore, it has been noted that the residual ion-motion-induced emittance growth can be mitigated by slice-by-slice matching the transverse phase space distribution of the witness bunch to the (nonlinear) ion-motion-perturbed wakefield[19].

Generating the tailored bunch profiles discussed in Ref. 19 using conventional beam shaping techniques is challenging. In this paper, we present a plasma-based scheme to generate the longitudinally shaped particle beams which are equilibrium solutions in the presence of ion motion.

The scheme relies on an adiabatic matching procedure where a witness bunch with, initially, longitudinally uniform transverse properties (i.e., untapered, with constant slice-by-slice size, emittance, and all other transverse phase-space properties) is injected into a PA stage operating in the blowout regime with a sufficiently low energy that ion motion effects are small. Assuming the witness bunch is initially matched in the unperturbed blowout wake (i.e., it propagates without transverse spot oscillations), its rms transverse size, σ_x, depends on the bunch's normalized rms emittance, ε_x, and energy, γmc^2 (m is the electron mass, c the speed of light in vacuum, and γ the bunch's relativistic Lorentz factor), according to

$$\sigma_x = \left(\frac{2\varepsilon_x^2}{k_p^2\gamma}\right)^{1/4}. \qquad (1)$$

Here $k_p = (4\pi n_0^2 q_e/mc^2)^{1/2}$ is the plasma wavenumber (n_0 is the background electron plasma density and q_e the electron charge). As shown in Ref. 19, background ion motion and the associated perturbation of the transverse (focusing) wakefield within the bunch itself become relevant when

$$\Lambda = Z_i \frac{m}{M_i}\frac{I_b}{I_A}\frac{L_b^2}{\sigma_x^2} \gtrsim 1. \qquad (2)$$

Here Z_i is the background ion charge state, M_i the ion mass, I_b is the bunch current, $I_A = mc^3/q_e \simeq 17$ kA is the Alfvén current, L_b is the bunch length (a top-hat longitudinal profile is considered), and the bunch is assumed to be round with a Gaussian transverse distribution. For this type of bunch, the ion-motion perturbed transverse wakefield is[19],

$$\frac{E_r - B_\theta}{E_0} = \frac{k_p r}{2}\left[1 + \Lambda\frac{\zeta^2}{L_b^2}H\left(\frac{r^2}{2\sigma_x^2}\right)\right], \qquad (3)$$

where E_r and B_θ are, respectively, the radial electric field and azimuthal magnetic field in the wake, $\zeta = z - ct$ is the longitudinal co-moving coordinate (z and t are, respectively, propagation distance and time; the bunch extends in the region $-L_b \le \zeta \le 0$, $\zeta = 0$ being the location of the bunch's head), r is the transverse coordinate, $E_0 = mc^2 k_p/q_e$, and $H(q) = (1 - e^{-q})/q$. The expression given by Eq. (3) is valid when ion motion is not too severe (i.e., $\Lambda < 1$). As a consequence of ion motion, the wake strength increases going from the head towards the tail of the bunch, and acquires a non-linear dependence from the transverse coordinate via the $H(r^2/2\sigma_x^2)$ term. From Eqs. (1) and (2) we see that $\Lambda \propto \gamma^{1/2}$, and so, as anticipated, ion-motion effects are less important at low energy.

For instance, for the PA-based LC design presented in Ref. 14, the parameters are $N_b = 10^{10}$, $L_b \simeq 20$ μm (yielding $I_b \simeq 24$ kA), $\varepsilon_x \simeq 0.6$ μm (round beam), and $n_0 \simeq 10^{17}$ cm^{-3}. At the proposed injection energy of 25 GeV, $\sigma_x \simeq 0.25$ μm, and so $\Lambda \simeq 5$ for a hydrogen ion background. We expect the head-to-tail wake perturbation from ion motion to be important in this case. However, for a much lower injection energy of, e.g., 50 MeV, we have $\sigma_x \simeq 1.2$ μm, yielding $\Lambda \simeq 0.2$, and so the perturbation from ion motion is small. Hence, for a sufficiently low bunch energy an untapered witness bunch can be (quasi-)matched in the (quasi-)unperturbed blowout wakefield (the smaller the ion motion perturbation, the better is the matching of the untapered witness bunch). When present, the resulting small initial mismatch, which grows from head to tail, is dissipated via phase mixing, and the bunch reaches an equilibrium state characterized by a slice-dependent (tapered) equilibrium size at the cost of a slight emittance growth which depends on the degree of wake perturbation at injection.

Note that the ion-motion-induced perturbation of the longitudinal wakefield is generally negligible. This can be seen using the Panofsky-Wenzel theorem, $\partial_\zeta(E_r - B_\theta) = \partial_r E_z$, where E_z is the longitudinal wake, from which we can estimate the degree of (maximum) wake perturbation at the tail of the bunch, which reads $|\delta E_z/E_0| \sim Z_i(m/M_i)\, k_p r_e N_b$ (here $r_e = q_e^2/mc^2 \simeq 2.81\cdot 10^{-13}$ cm is the classical electron radius). For collider-relevant bunch parameters in a hydrogen plasma with $n_0 = 10^{17}$ cm^{-3}, we obtain $|\delta E_z/E_0| \sim 10^{-3}$.

As the witness bunch accelerates, its transverse size is adiabatically reduced (adiabatic compression). The increasing bunch density gradually triggers ion motion and wakefield perturbation, but since changes in the bunch distribution due to the acceleration generally occur over a longer time scale than the betatron motion, the witness bunch transverse phase-space distribution at each location along the beam remains matched in the wake-

field. This implies that, as the bunch readjusts itself during acceleration (e.g., the bunch slices towards the tail evolve more, resulting in their transverse size to shrink more, compared to the ones closer to the head, owing to the increasing amount of ion-motion induced wake perturbation developing during acceleration), the equilibrium slice emittance (defined as the rms transverse phase-space area at each longitudinal slice) is essentially preserved. On the other hand, as a result of the tapered shape being acquired by the bunch, the projected emittance (defined as the rms transverse phase-space area for the whole beam) slowly grows during acceleration and saturates at high energy. By accelerating the bunch maintaining every slice in a state of equilibrium, the adiabatic matching procedure delivers a high-energy witness bunch with a longitudinally tapered profile that is slice-by-slice nonlinearly matched to the ion-motion-perturbed wakefield.

The proposed matching method is conceptually simpler than the one discussed in in Ref. 26, where the emittance growth problem associated with ion motion was addressed by considering an adiabatic matching region, located at the entrance of the PA stage, consisting of a plasma section realized with several different ion species arranged in layers of decreasing ion mass.

Even though the adiabatic matching method is being proposed and analyzed in the context of ion motion, it can be used to generate equilibrium bunch profiles in all cases where the focusing force acting on the witness bunch is nonlinear, slice-dependent, and changes slowly with energy (i.e., changes in the wake are small over a betatron period), provided that for a low enough energy a state exists where such forces are uniform along the bunch and the nonlinearity is small.

The paper is organized as follows. The adiabatic matching procedure is presented in detail in Sec. II. An application of the method in the case of collider-relevant witness bunch parameters, where the conditions required to achieve a complete adiabatic matching might not always be fulfilled, is discussed in Sec. III. A moments-based, analytical description of the matching process addressing the slow (secular) emittance growth associated with the matching process itself is presented in Sec. IV. Finally, conclusions are presented in Sec. V.

All the simulation results presented in this paper have been obtained with the quasi-static modality of the Particle-In-Cell (PIC) code INF&RNO[27–29]. In order to correctly resolve ion motion dynamics in the vicinity of the witness bunch, the code has been equipped with a high resolution computational sub-grid similar to the one first implemented in the PIC code HiPACE[30] and discussed in Ref. 31.

II. ADIABATIC MATCHING OF BEAMS IN THE ION-MOTION PERTURBED WAKEFIELD

We will discuss the concept of adiabatic matching for a witness bunch injected in a PA stage operating in the blowout regime. Extension of the concept to other PA regimes is straightforward. In all the examples considered in this work the PA stage is driven by a Gaussian electron drive beam with a peak density of $n_b^{(d)}/n_0 = 4$, rms transverse sizes $\sigma_x^{(d)} = \sigma_y^{(d)} = 0.8 k_p^{-1}$, and rms length $\sigma_z^{(d)} = \sqrt{2} k_p^{-1}$. The background plasma is hydrogen with density $n_0 = 10^{17}\mathrm{cm}^{-3}$. For simplicity, we assume that the driver is moving at the speed of light and is non-evolving.

We consider a witness bunch with a length $L_b = 2\ k_p^{-1} \simeq 33.4\ \mu$m, and a trapezoidal current profile ranging from $I_{b,head} \simeq 27.2$ kA at the head to $I_{b,tail} \simeq 17.6$ kA at the tail (the total number of particles in the bunch is $N_b \simeq 1.6 \cdot 10^{10}$). The witness bunch head is located at a distance of $\simeq 5\ k_p^{-1} \simeq 83.5\ \mu$m behind the center of the drive beam such that the blowout wake is optimally loaded[32], generating a constant longitudinal electric field along the witness bunch, $E_{z,b}$, so that the energy gain is $k_p^{-1} d\gamma/dz = -E_{z,b}/E_0 \simeq 0.564$ for all beam slices. The bunch has a transverse Gaussian distribution and is initially untapered, i.e., the rms bunch size is constant along the bunch. We assume, for simplicity, the bunch to be round, but adiabatic matching of flat beams is also possible. Finally, we chose the initial bunch normalized emittance to be $\varepsilon_{x,0} = 1$ mm mrad.

A. Condition for adiabatic matching.

The adiabatic matching procedure provides a way of generating a nonlinearly matched, longitudinally tapered witness bunch that is an equilibrium solution in the presence of ion motion starting from a bunch that has, initially, an untapered, longitudinally uniform transverse structure. The method requires injecting the witness bunch in the PA stage with, initially, a transverse size large enough that the space charge forces associated with the bunch itself do not significantly perturb the ion distribution on a time scale comparable with the bunch duration, and so the transverse wake remains longitudinally uniform and changes linearly with the transverse coordinate. In this case, the untapered bunch can be (quasi-)matched to the (quasi-)unperturbed wakefield. Following Eq. (2), and owing to the relation between bunch size, energy, and emittance, given by Eq. (1) for a PA stage operating in the blowout regime, the requirement of a large enough initial witness bunch size implies choosing a low enough injection energy γ_i such that $\Lambda \ll 1$, and so

$$\gamma_i \ll \tilde{\gamma}_i \equiv 2 \left(\frac{1}{Z_i} \frac{M_i}{m} \frac{I_A}{I_b} \frac{\varepsilon_{x,0}}{k_p L_b^2} \right)^2 . \tag{4}$$

Note that Eq. (4) was derived assuming a bunch with constant longitudinal current profile. For a bunch, as in this case, with a trapezoidal current profile we can assume $I_b \approx (I_{b,head} + I_{b,tail})/2$. Equation (4) suggests that, as expected, adiabatic matching is easier to realize in case of heavier background ions and shorter bunches. However, the use of heavy ions is not, in general, desirable since, unless they are completely ionized, the multiple ionization states available could lead to uncontrolled plasma formation within the bunch owing to the large space-charge fields associated with the bunch itself, resulting in the degradation of the wakefield and, hence, emittance growth[33].

For the witness bunch parameters considered here Eq. (4) indicates that an injection energy below ~ 440 MeV (the lower the better) is low enough that, at least initially, ion-motion-induced wake perturbation is small. Hence, to illustrate the adiabatic matching procedure we chose an injection energy of 50 MeV, yielding $\sigma_x \simeq 1.5$ μm, and $\Lambda \simeq 0.3$.

Figure 1(a) shows a two-dimensional (2D) (ζ, x) map of the transverse wakefield in the region of the witness bunch at injection (50 MeV bunch energy) from an INF&RNO simulation. The bunch rms envelope is shown in green. The numerical parameters used in this and all the other PIC simulations presented in this work are as follows. Simulations are performed in 2D axisymmetric geometry, where we used a (ζ, r) computational box (main grid) with dimensions $13.2 \times 10\ k_p^{-2}$. The longitudinal cell size was $0.0125\ k_p^{-1}$, the transverse cell size was defined in terms of the witness bunch transverse size at injection and was equal to $\sigma_x/10$. In the witness beam region we used a higher resolution subgrid[31] with dimensions $2.1 \times 1.5\ k_p^{-2}$, longitudinal cell size of $0.005 k_p^{-1}$, and transverse cell size $\sigma_x/18$. The witness beam was sampled with 10^6 numerical particles. Witness beam particles are pushed in 3D. In the main grid plasma electrons are sampled with 4 particles per cell (p.p.c.), ions are immobile (static background). In the subgrid there are no plasma electrons, plasma ions are sampled with 2 p.p.c. The adaptive temporal evolution step is defined in terms of the (energy-dependent) betatron period of the witness bunch and was set to 40 steps per betatron period. A 10-fold sub-cycling is also used for every witness particle push.

The wake in Fig. 1(a) appears longitudinally uniform and, as expected, ion-motion-induced effects are small. This is confirmed by Fig. 2 where we plot (solid black line) a transverse lineout of the wakefield taken at the tail of the bunch ($\zeta = -L_b$). Compared to the unperturbed wakefied (dotted black line), the focusing gradient is slightly enhanced (by approximately $\sim 42\%$, qualitatively consistent with the estimate given by Eq. (3)), and the amount of mismatch, defined as the ratio of the injected witness bunch size to the actual matched bunch size (a value of one indicates no mismatch), is $\simeq 1.09$. Note that the tail of the bunch is the region where the mismatch is the largest. For instance, in the bunch center ($\zeta = -L_b/2$) the amount of mismatch is only $\simeq 1.02$, and vanishes at the head of the bunch. When present, this small initial mismatch is eliminated via phase mixing (because of its slice-dependent nature and nonlinear component of the ion-motion-perturbed wakefield), and the witness bunch reaches an equilibrium state characterized by a slice-dependent equilibrium size at a price of a slight emittance growth. However, since the amount of mismatch at injection is generally small, the equilibrium state is a perturbation of the initial one.

B. (Quasi-)preservation of witness bunch slice emittance during adiabatic acceleration.

During acceleration the witness bunch is compressed transversely [see Eq. (1)], and the increasing bunch density triggers ion motion and the associated wakefield perturbation. This is shown in Fig. 1(b), (c), and (d), where we plot the 2D maps of the transverse wakefield and the corresponding rms bunch envelopes when the bunch energy is 1.05 GeV [$\Delta\gamma mc^2 = (\gamma - \gamma_i)mc^2 = 1$ GeV energy gain] (b), 2.05 GeV ($\Delta\gamma mc^2 = 2$ GeV energy gain) (c), and 10.05 GeV ($\Delta\gamma mc^2 = 10$ GeV energy gain) (d). Transverse lineouts of the wakefield at the tail of the bunch for the three bunch energies are shown in Fig. 2 (red, green, and blue lines, respectively). The increased degree of wake perturbation from ion motion (from mild to severe) as the bunch energy increases is evident. Note that during this process the ion distribution, which is initially cold, remains cold. As previously noted, ion motion effects become more relevant towards the tail of the bunch (increased focusing gradient). However, changes to the beam distribution due to acceleration generally happen over a time scale longer than the one characterizing the transverse particle dynamics (i.e., betatron motion), hence the evolution of the witness bunch in the changing wakefield is adiabatic. In fact, the characteristic length scale of beam evolution due to acceleration, L_{acc}, is given by

$$L_{acc}^{-1} \simeq \frac{1}{n_b}\frac{\partial n_b}{\partial z}\bigg|_{acc} \simeq \frac{k_p}{2\gamma}\frac{|E_{z,b}|}{E_0}, \qquad (5)$$

where $n_b \propto N_b/(\sigma_x^2 L_b)$ is the witness beam density, while the betatron period scales as $k_\beta \sim k_p/\gamma^{1/2}$, and so $k_\beta L_{acc} \sim \gamma^{1/2}/(|E_{z,b}|/E_0) \gg 1$. The consequence of adiabaticity is that the bunch phase space distribution, which is in equilibrium as soon as the mismatch present at injection is dissipated, remains matched to the evolving wakefield even when ion motion becomes severe, and the slice emittance is essentially preserved. This is shown in Fig. 3, where we plot the slice emittance (normalized to $\varepsilon_{x,0}$) for different values of the bunch energy during acceleration, namely 50 MeV (i.e., at injection, black line), 1.05 GeV ($\Delta\gamma mc^2 = 1$ GeV energy gain, red line), 2.05 GeV ($\Delta\gamma mc^2 = 2$ GeV energy gain, green line) curve, and 10.05 GeV ($\Delta\gamma mc^2 = 10$ GeV energy gain, blue line). The slice emittance is overall well conserved, acquiring

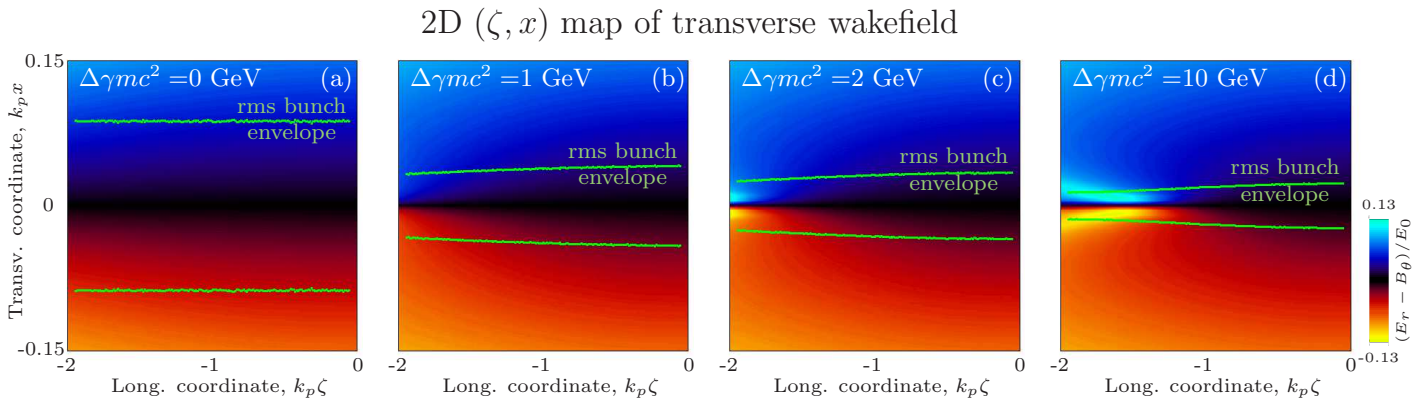

FIG. 1. Two-dimensional (ζ, x) maps of the transverse wakefield in the region of the witness bunch, and corresponding rms bunch envelopes (green lines) for different values of the bunch energy during acceleration, namely at injection [$\gamma_i mc^2 = 50$ MeV, $\Delta\gamma mc^2 = (\gamma - \gamma_i)mc^2 = 0$ GeV] (a), and for $\Delta\gamma mc^2 = 1$ GeV (b), $\Delta\gamma mc^2 = 2$ GeV (c), and $\Delta\gamma mc^2 = 10$ GeV (d).

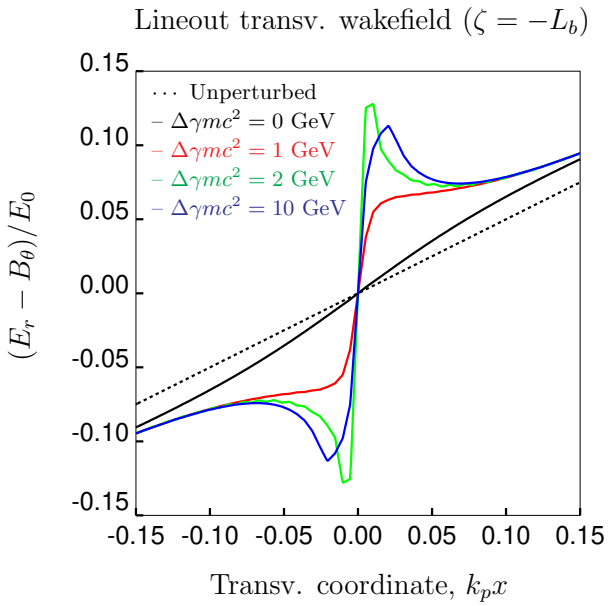

FIG. 2. Transverse lineout of the transverse wakefield, $(E_r - B_\theta)/E_0$, taken at the tail of the witness bunch ($\zeta = -L_b$) for different values of the bunch energy during acceleration, namely at injection [$\gamma_i mc^2 = 50$ MeV, $\Delta\gamma mc^2 = (\gamma - \gamma_i)mc^2 = 0$ GeV] (solid black line), and for $\Delta\gamma mc^2 = 1$ GeV (solid red line), $\Delta\gamma mc^2 = 2$ GeV (solid green line), and $\Delta\gamma mc^2 = 10$ GeV (solid blue line). The unperturbed wakefield is indicated by the black dotted line.

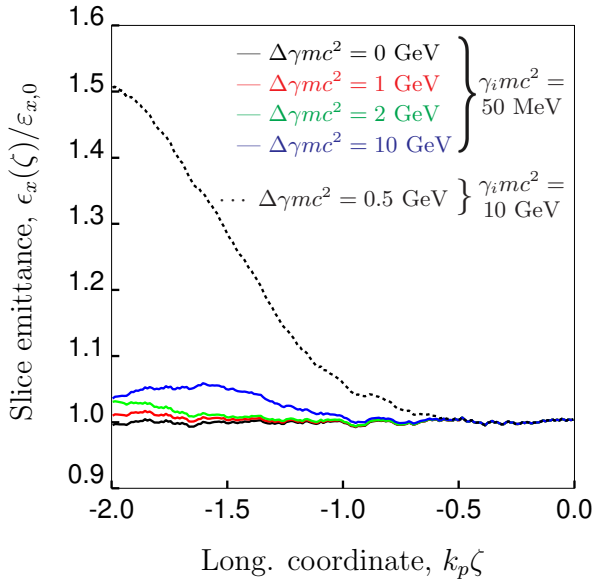

FIG. 3. Slice emittance (normalized to $\varepsilon_{x,0} = 1$ μm) for different values of the witness bunch energy during acceleration, namely at injection ($\gamma_i mc^2 = 50$ MeV, $\Delta\gamma mc^2 = (\gamma - \gamma_i)mc^2 = 0$ GeV) (solid black line), and for $\Delta\gamma mc^2 = 1$ GeV (solid red line), $\Delta\gamma mc^2 = 2$ GeV (solid green line), and $\Delta\gamma mc^2 = 10$ GeV (solid blue line). The black dotted line is the slice emittance for a bunch injected with a 10 GeV energy after a propagation distance yielding a 0.5 GeV energy gain.

only a slight head to tail chirp ($\sim 5\%$ emittance increase towards the tail). For comparison, the black dotted line is the slice emittance for a bunch injected with a 10 GeV energy after a propagation distance yielding a 0.5 GeV energy gain. In this case without adiabatic matching the slice emittance is severely degraded ($\sim 50\%$ emittance increase towards the tail).

By accelerating the witness bunch maintaining every slice in a state of equilibrium, the adiabatic matching procedure delivers, starting from a low-energy, initially untapered bunch, a high-energy bunch with a longitudinally tapered transverse profile that is, slice-by-slice, nonlinearly matched to the ion-motion-perturbed wakefield. This is done (quasi-)preserving the slice emittance.

In Fig. 4 we show snapshots of the particle witness bunch distribution at injection (50 MeV, untapered) (a),

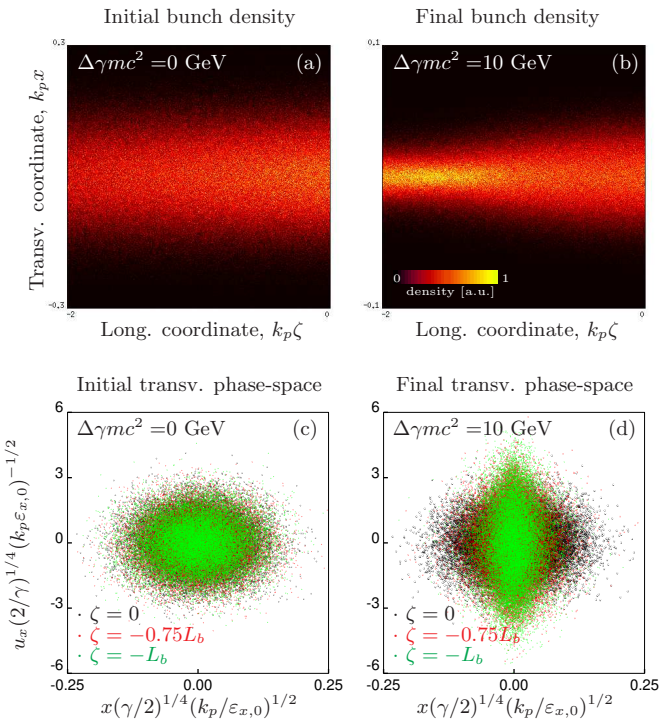

FIG. 4. Witness bunch density distribution at injection ($\gamma_i mc^2$ = 50 MeV, $\Delta\gamma mc^2$ = 0 GeV) (a), and after a $\Delta\gamma mc^2$ = 10 GeV energy gain with adiabatic matching (b). Transverse phase-space, (x, u_x), at injection (c) and after a 10 GeV energy gain. In order to directly compare phase spaces obtained at different energies particle positions and momenta have been rescaled with $(2/\gamma)^{1/4}(\varepsilon_{x,0}/k_p)^{1/2}$ and $(\gamma/2)^{1/4}(k_p\varepsilon_{x,0})^{1/2}$, respectively. For clarity, only particles belonging to slices at the head ($\zeta = 0$, black dots), mid-rear section ($\zeta = -0.75 \cdot L_b$, red dots), and tail ($\zeta = -L_b$, green dots) of the bunch have been plotted.

and after a $\Delta\gamma mc^2 = 10$ GeV energy gain with adiabatic matching. The tapered profile in Fig. 4 (b) corresponds to one of the (infinitely many) stationary Maxwell-Vlasov equilibrium solutions described in Ref. 19. This is shown in Fig. 5, where we compare the slice-dependent rms bunch radius for the bunch shown in Fig. 4 (b) (black line) to that of a 10.05 GeV equilibrium bunch from Ref. 19 (red dashed line) that has the same longitudinal current distribution, the same slice emittance, and the same transverse distribution for $\zeta = 0$ (i.e., at the bunch head) of the bunch undergoing adiabatic matching. Note that, in general, the final bunch distribution delivered by adiabatic matching depends on the choice of the initial (injected) bunch distribution, and so multiple final equilibrium distributions are possible.

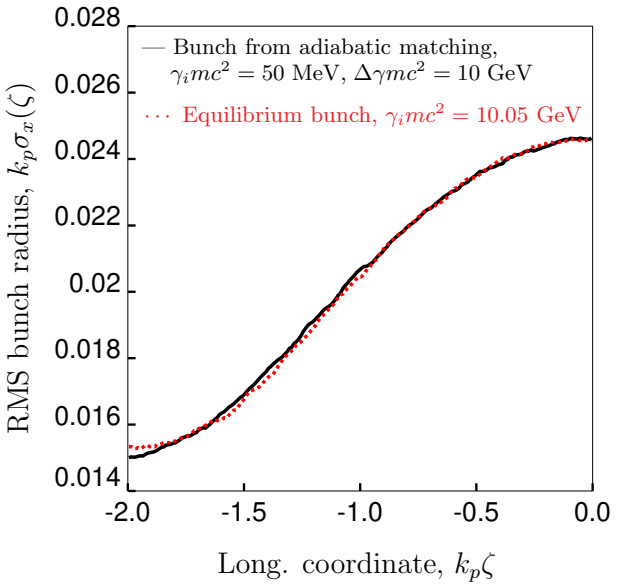

FIG. 5. Comparison of the slice-dependent rms bunch radius for the bunch shown in Fig. 4 (b) (black line) to that of a 10.05 GeV equilibrium bunch from Ref. 19 (red dashed line) that has the same longitudinal current distribution, the same slice emittance, and the same transverse distribution for $\zeta = 0$ (i.e., at the bunch head) of the bunch undergoing adiabatic matching.

C. Growth of projected bunch witness emittance during adiabatic matching.

Even though the slice emittance is (quasi-)preserved during adiabatic matching, the projected witness bunch emittance displays a slow (secular) growth. This is shown in Fig. 6, where the solid black line is the emittance evolution (normalized to $\varepsilon_{x,0}$) for the bunch undergoing adiabatic matching plotted as a function of the propagation distance in the PA stage. The solid green line shows the same quantity for a bunch injected with 10 GeV energy. In both cases, the long term evolution of the emittance (i.e., after mixing has occurred in the non-adiabatic injection case) shows a slow growth with a growth rate that decreases at high energy. Note that without acceleration (i.e., if bunches are propagating in an ion channel) no secular emittance growth is observed[19]. Also, no significant change in emittance is observed with acceleration and without ion motion (we recall that our bunches have zero energy spread at injection, and optimal beamloading is used to avoid growth of energy spread during acceleration). Hence, the secular emittance growth is triggered by ion motion and depends on acceleration.

In order to further investigate the source of this growth, we run two additional simulations using witness beams that are, from the start, equilibrium solutions in the presence of ion motion, as described in Ref. 19. The chosen injection energies were 50 MeV (red dotted line) and 10 GeV (blue dotted line). Note that the (ini-

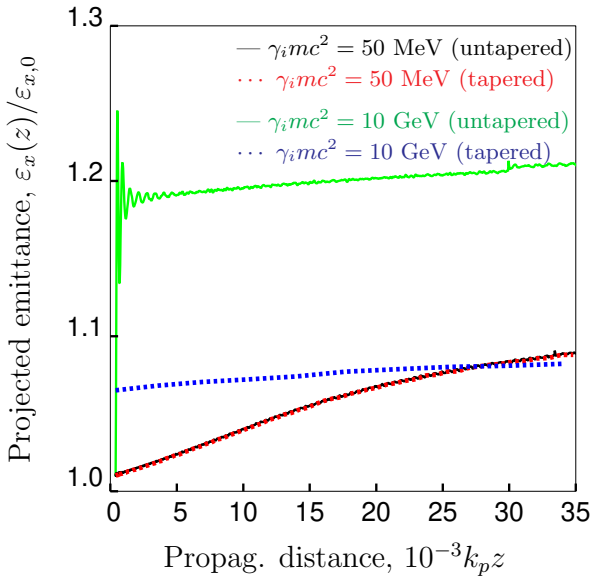

FIG. 6. Evolution of the projected witness bunch emittance (normalized to $\varepsilon_{x,0} = 1$ μm) for an untapered bunch injected with $\gamma_i mc^2 = 50$ MeV (solid black line) and $\gamma_i mc^2 = 10$ GeV (solid green line). Evolution of the emittance for a longitudinally tapered, equilibrium bunch injected with $\gamma_i mc^2 = 50$ MeV (dotted red line) and $\gamma_i mc^2 = 10$ GeV (dotted blue line). The propagation distance corresponds to a $\Delta\gamma mc^2 = 10$ GeV energy gain.

tial) slice emittance is the same for all beams ($\varepsilon_{x,0} = 1$ μm). However, equilibrium beams are longitudinally tapered hence, the projected emittance differs from the slice emittance. This is particularly evident in the case of the 10 GeV equilibrium beam, for which the tapering is more severe. As expected, there is no emittance growth from ion-motion induced mismatch for the equilibrium bunches. However, a secular growth is present and the rate of growth for both injection energies is the same as in their corresponding initially untapered cases (e.g., compare solid black line vs dotted red line, and solid green line vs dotted blue line in Fig. 6). Hence, this shows that the secular growth is not associated with the mismatch of an initially untapered bunch, but, instead, it is related to the ion-motion-induced tapering acquired by the bunch itself during acceleration.

In fact, as the witness bunch accelerates ion-motion effects increase, but, as pointed out earlier, the amount of transverse wake perturbation changes slice-by-slice, and the slices towards the tail of the bunch are the ones experiencing the strongest evolution. This uneven rate of transverse evolution for the different slices is the cause of the growth of the projected emittance. This is shown in Fig. 4 (c) and (d), where we plot the (x, u_x) transverse phase-space (x it the transverse particle position, u_x is the transverse particle momentum normalized to mc) for the bunch undergoing adiabatic matching. In order to directly compare phase spaces obtained at different energies particle positions and momenta have been rescaled with $(2/\gamma)^{1/4}(\varepsilon_{x,0}/k_p)^{1/2}$ and $(\gamma/2)^{1/4}(k_p\varepsilon_{x,0})^{1/2}$, respectively. The plot in (c) is at injection, the one in (d) after a 10 GeV energy gain. For clarity, only particles belonging to slices at the head ($\zeta = 0$, black dots), mid-rear section ($\zeta = -0.75 \cdot L_b$, red dots), and tail ($\zeta = -L_b$, green dots) of the bunch have been plotted. The increase of the (projected) phase-space area occupied by the bunch as a consequence of the non-uniform evolution of the different slices is evident. We will explore quantitatively this aspect in Sec. IV by using a moments description for the witness bunch.

III. GENERATION OF MATCHED BEAMS IN THE PRESENCE OF ION MOTION FOR COLLIDER-RELEVANT WITNESS BUNCH PARAMETERS

In this section, we analyze the performance of the matching scheme discussed in the previous section from the point of view of emittance preservation in the case of electron witness bunches with a collider-relevant emittance. All the bunch and plasma parameters considered in this section are as in Sec. II, except for the initial emittance, for which we consider the value $\varepsilon_{x,0} = 0.2$ μm. As before, we consider for simplicity an axisymmetric (round) bunch. Note that several LC designs consider beams with asymmetric emittances (i.e., flat beams) to minimize beamstrahlung effects[34]. In this case, the emittances in the horizontal and vertical planes are $\sim \mu$m and ~ 10 nm, respectively, and the geometric average of the two is ~ 0.1 μm, comparable with the value chosen in the symmetric case. Simulations and theory show that from the point of view of ion motion effects, the emittance evolution in the (much simpler to model) symmetric case is representative of the evolution of the geometric average of the emittances in the asymmetric case[19,20].

For a bunch with collider-relevant parameters Eq. (4) gives $\tilde{\gamma}_i \simeq 35$. However, an injection energy (much) lower than $\simeq 18$ MeV could be impractical because of, e.g., potential beam quality degradation from space-charge effects, or dispersion in case the bunch has a finite energy spread and/or energy chirp. Hence, in this case, it is not possible to operate in a regime where, at injection, $\Lambda \ll 1$. However, owing to the weak energy scaling of ion-motion-induced wakefield perturbations ($\Lambda \propto \gamma^{1/2}$), we expect that operating at a relatively low energy, even though higher than $\sim \tilde{\gamma}_i mc^2$, will nonetheless prove to be beneficial in reducing the emittance degradation associated with ion motion effects compared to cases where the injection energy is at the 10s of GeV level[3,14]. In the following, we quantitatively explore the role of injection energy by means of computer simulations.

In Fig. 7(a), we show the evolution of the projected bunch emittance (normalized to $\varepsilon_{x,0}$) as a function of the propagation distance in the PA stage for different values of the injection energy, namely $\gamma_i mc^2 = 50$ MeV ($\Lambda \simeq 1.7$ at injection, black line), $\gamma_i mc^2 = 100$ MeV ($\Lambda \simeq$

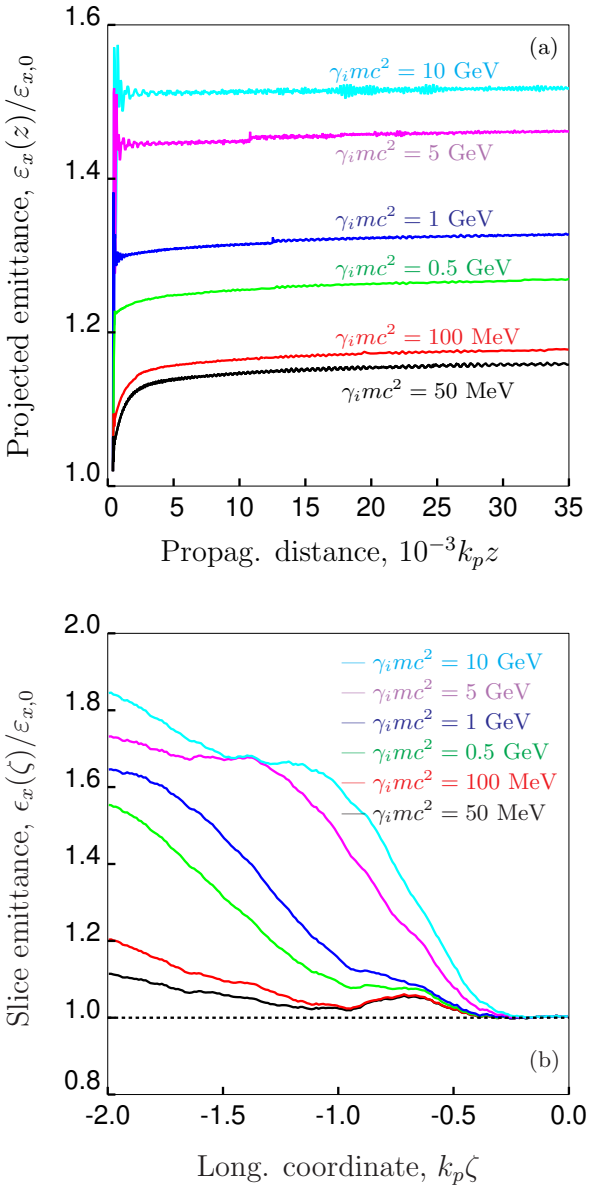

FIG. 7. Evolution (a) of the projected witness bunch emittance (normalized to $\varepsilon_{x,0} = 0.2$ μm) as a function of the propagation distance in the PA stage for different values of the injection energy, namely $\gamma_i mc^2 = 50$ MeV ($\Lambda \simeq 1.7$ at injection, black line), $\gamma_i mc^2 = 100$ MeV ($\Lambda \simeq 2.4$, red line), $\gamma_i mc^2 = 0.5$ GeV ($\Lambda \simeq 5.3$, green line), $\gamma_i mc^2 = 1$ GeV ($\Lambda \simeq 7.5$, blue line), $\gamma_i mc^2 = 5$ GeV ($\Lambda \simeq 17$, purple line), and $\gamma_i mc^2 = 10$ GeV ($\Lambda \simeq 23$, cyan line). The propagation distance corresponds to a 10 GeV energy gain. Bunch slice emittance (b) after a $\Delta\gamma mc^2 = 10$ GeV energy gain for the different values of the injection energy listed earlier.

2.4, red line), $\gamma_i mc^2 = 0.5$ GeV ($\Lambda \simeq 5.3$, green line), $\gamma_i mc^2 = 1$ GeV ($\Lambda \simeq 7.5$, blue line), $\gamma_i mc^2 = 5$ GeV ($\Lambda \simeq 17$, purple line), and $\gamma_i mc^2 = 10$ GeV ($\Lambda \simeq 23$, cyan line). We see that for an injection energy $\lesssim 100$ MeV, even though $\Lambda \gtrsim 1$, the initial emittance degradation is small. Indeed, the growth associated with mismatch at injection is smaller than the (intrinsic) secular growth due to bunch readjustment during acceleration, which saturates at $\sim 15\%$. This is not the case for injection energies above 100 MeV, where the emittance growth is dominated by bunch mismatch at injection. In Fig. 7(b) we show the bunch slice emittance after a 10 GeV energy gain for the different values of the injection energy listed earlier. For a 50 MeV injection energy the slice emittance degradation (tapering) is $\lesssim 10\%$, but reaches $\sim 85\%$ for a 10 GeV injection energy.

IV. BEAM-MOMENTS-BASED ANALYTICAL DESCRIPTION OF THE MATCHING PROCESS

In this section, we present a moments-based description for the witness bunch to model the growth of the projected emittance during adiabatic matching. The results in this section are partially based on the work described in Refs. 19 and 25.

We consider a relativistic electron bunch with a (radially symmetric) density profile parametrized as

$$n_b(\zeta, r; z) = n_{b,0}\, g_\parallel(\zeta) g_\perp(r; \zeta; z), \tag{6}$$

where $n_{b,0}$ is the initial peak density, $g_\parallel(\zeta)$ and $g_\perp(r; \zeta; z)$ describe, respectively, the longitudinal and the $\zeta-$dependent transverse profile of the bunch. Note that $g_\perp$ changes as a function of the propagation distance, z, during acceleration. We recall that the bunch head is located at $\zeta = 0$ and that the bunch extends for $\zeta < 0$. We require that, for any longitudinal slice and propagation distance,

$$\int_0^\infty g_\perp(r; \zeta; z)\, r dr = \int_0^\infty g_\perp(r; \zeta = 0; z = 0)\, r dr, \tag{7}$$

so that the bunch current density profile only depends on the choice of $g_\parallel(\zeta)$, and this can be arbitrary. The ion-motion-perturbed transverse wakefield for a PA stage operating in the blowout regime is[19]

$$\frac{E_r - B_\theta}{E_0} = \frac{k_p r}{2} + Z_i \frac{m}{M_i} \frac{n_{b,0}}{n_0} \frac{k_p^3}{r} \int_\zeta^\infty d\zeta'(\zeta' - \zeta) g_\parallel(\zeta') \times \int_0^r g_\perp(r'; \zeta'; z) r' dr'. \tag{8}$$

Equation (8) is valid when ion perturbation is not too large. Assuming a (slice-dependent) transverse Gaussian distribution, and imposing the condition expressed in Eq. (7), we have

$$g_\perp(r; \zeta; z) = \frac{\sigma_0^2}{\sigma^2(\zeta; z)} \exp\left[-\frac{r^2}{2\sigma^2(\zeta; z)}\right], \tag{9}$$

where $\sigma(\zeta; z)$ is the slice- and propagation-dependent rms transverse bunch size, and $\sigma_0 = \sigma(\zeta = 0; z = 0)$, where $z = 0$ represents the initial condition. For the trapezoidal current profile (optimal beamloading) as the one

considered in this paper (see Sec. II), we have

$$\frac{n_{b,0}}{n_0} = \frac{2}{(k_p\sigma_0)^2}\frac{I_{b,head}}{I_A}, \tag{10}$$

and

$$g_\parallel(\zeta) = 1 + \left(1 - \frac{I_{b,tail}}{I_{b,head}}\right)\frac{\zeta}{L_b}, \tag{11}$$

for $-L_b \le \zeta \le 0$, and $g_\parallel(\zeta) = 0$ elsewhere. Inserting Eq. (9) into Eq, (8), and using Eq. (10), we obtain

$$\frac{E_r - B_\theta}{E_0} = \frac{k_p r}{2}\left[1 + 2Z_i\frac{m}{M_i}\frac{I_{b,head}}{I_A} \times \int_\zeta^\infty d\zeta'(\zeta'-\zeta)\frac{g_\parallel(\zeta')}{\sigma^2(\zeta';z)}H\left(\frac{r^2}{2\sigma^2(\zeta';z)}\right)\right], \tag{12}$$

where H is the function defined in Sec. I.

From the expression of the wakefield given in Eq. (12) we can derive the average betatron wavenumber in any slice along the bunch (and for a given propagation distance) according to

$$k_\beta^2(\zeta;z) = \frac{k_p\langle r(E_r - B_\theta)\rangle}{E_0\gamma\langle r^2\rangle}, \tag{13}$$

where the slice averaging is defined according to the bunch phase-space distribution. For instance, the spatial average is defined via $g_\perp$ as

$$\langle f\rangle = \frac{\int_0^\infty f(r)g_\perp(r;\zeta;z)rdr}{\int_0^\infty g_\perp(r;\zeta;z)rdr}, \tag{14}$$

and where $f(r)$ is any arbitrary function. We obtain

$$k_\beta^2(\zeta;z) = k_{\beta,0}^2[1+\lambda(\zeta;z)], \tag{15}$$

where $k_{\beta,0}^2 = k_p^2/2\gamma$ is the unperturbed betatron wavenumber in a blowout wake, and the contribution from ion motion is

$$\lambda(\zeta;z) = 2Z_i\frac{m}{M_i}\frac{I_{b,head}}{I_A}\int_\zeta^\infty \frac{(\zeta'-\zeta)g_\parallel(\zeta')}{\sigma^2(\zeta;z)+\sigma^2(\zeta';z)}d\zeta' \ge 0. \tag{16}$$

The condition that ion motion must not be too severe in order for this analytic treatment to be valid requires operating in regimes where $\lambda < 1$.

The introduction of the $\zeta-$dependent average betatron wavenumber makes it possible to capture the slice-dependent nature of ion-motion-induced wakefield perturbation (i.e., enhancement of the wakefield strength going form the head to the tail of the bunch). We recall that ion motion also causes the wakefield to acquire a nonlinear component from the transverse coordinate. This effect introduces an in-slice spread of betatron frequencies (i.e., particle with different betatron amplitudes have different betatron periods). However, at least when ion motion is not too severe, head-to-tail effects are the dominant ones. Hence, we neglected contributions from nonlinearities in the moments description of the matching process. By neglecting the nonlinearity we can assume that for each slice the bunch density distribution remains Gaussian at all times, and the slice emittance is preserved, while growth of the projected emittance can occur as a consequence of different slices evolving at different rates.

With the aforementioned assumptions, and by averaging the single particle equations of motion for a generic witness bunch particle (i.e., $dx/dz = u_x/\gamma$, $du_x/dz = -\gamma k_\beta^2 x$) over the bunch phase-space distribution, we obtain the equations for the $\zeta-$dependent, second-order phase-space moments of the bunch describing the evolution of each slice, which read

$$\frac{\partial\langle x^2\rangle}{\partial z} = \frac{2}{\gamma}\langle xu_x\rangle, \tag{17a}$$

$$\frac{\partial\langle xu_x\rangle}{\partial z} = \frac{\langle u_x^2\rangle}{\gamma} - \frac{k_p^2}{2}(1+\lambda)\langle x^2\rangle, \tag{17b}$$

$$\frac{\partial\langle u_x^2\rangle}{\partial z} = -k_p^2(1+\lambda)\langle xu_x\rangle. \tag{17c}$$

In deriving the equations we assumed there is zero initial energy spread, and the energy of all slices evolves as

$$\gamma = \gamma_i + \gamma' z, \tag{18}$$

where $\gamma' = -k_p E_{z,b}/E_0$. Also, the witness bunch is assumed to be relativistic, $\gamma_i \gg \langle u_x^2\rangle$. We recall that the bunch is symmetric, and so the evolution in the (x,u_x) and (y,u_y) transverse phase-space planes is identical. Note that $\sigma^2 = \langle x^2\rangle$, and, hence, the equations for different slices (i.e., different values of ζ) are coupled via ion motion (i.e., the λ term given by Eq. (16)).

The (squared) slice normalized emittance of the bunch is defined as $\epsilon_x^2 = \langle x^2\rangle\langle u_x^2\rangle - \langle xu_x\rangle^2$. One can easily verify that Eq. (17) implies that the slice emittance is preserved. Evaluating the projected bunch emittance requires longitudinally averaging the second-order moments. The averaging is defined via $g_\parallel$ as

$$\overline{h} = \frac{\int_{-\infty}^{+\infty} h(\zeta)g_\parallel(\zeta)d\zeta}{\int_{-\infty}^{+\infty} g_\parallel(\zeta)d\zeta}, \tag{19}$$

where h stands for $\langle x^2\rangle$, $\langle xu_x\rangle$, or $\langle u_x^2\rangle$. The (squared) projected emittance is then $\varepsilon_x^2 = \overline{\langle x^2\rangle}\,\overline{\langle u_x^2\rangle} - \overline{\langle xu_x\rangle}^2$.

As initial condition we consider an untapered bunch at focus linearly matched in the unperturbed wakefield ($\varepsilon_{x,0}$ is the initial normalized emittance), namely

$$\langle x^2\rangle(\zeta;z=0) = \sigma_0^2 = \sqrt{\frac{2}{\gamma_i}}\frac{\varepsilon_{x,0}}{k_p}, \tag{20a}$$

$$\langle xu_x\rangle(\zeta;z=0) = 0, \tag{20b}$$

$$\langle u_x^2\rangle(\zeta;z=0) = \sqrt{\frac{\gamma_i}{2}}k_p\varepsilon_{x,0}. \tag{20c}$$

It is evident that the initial condition given in Eq. (20) is not a stationary solution of Eq. (17). This is due, as we

know, to ion motion that induces a longitudinal variation of the transverse focusing force, described by the λ term, that at injection can be written as

$$\lambda(\zeta; z=0) \equiv \lambda_i(\zeta) = Z_i \frac{m}{M_i}\sqrt{\frac{\gamma_i}{2}}\frac{k_p}{\epsilon_{x,0}}\frac{\zeta^2}{2} \times \frac{I_{b,head} + \frac{1}{3}\left(I_{b,head} - I_{b,tail}\right)\frac{\zeta}{L_b}}{I_A}. \quad (21)$$

In order to assess the degree of mismatch we need to compute the bunch profile corresponding to a stationary equilibrium solution of Eq. (17). This is done by setting $\partial_z\langle x^2\rangle = 0$, $\partial_z\langle x u_x\rangle = 0$, $\partial_z\langle u_x^2\rangle = 0$ in Eq. (17), and using the constraint that the slice emittance is slice-by-slice constant and equal to $\varepsilon_{x,0}$. One finds that the equilibrium solution, valid for a generic bunch energy, is given by

$$\langle x^2\rangle_{eq}(\zeta) = \sqrt{\frac{2}{\gamma}}\frac{\varepsilon_{x,0}}{k_p}\frac{1}{\sqrt{1+\lambda_{eq}(\zeta)}}, \quad (22a)$$

$$\langle x u_x\rangle_{eq}(\zeta) = 0, \quad (22b)$$

$$\langle u_x^2\rangle_{eq}(\zeta) = \sqrt{\frac{\gamma}{2}}k_p\varepsilon_{x,0}\sqrt{1+\lambda_{eq}(\zeta)}, \quad (22c)$$

where λ_{eq} is given by Eq. (16) evaluated using $\langle x^2\rangle_{eq}$. Hence, Eq. (22a) defines $\langle x^2\rangle_{eq}$ implicitly. Equation (22a) can be easily solved numerically in a recursive way starting from the bunch's head, where $\lambda_{eq}(\zeta = 0) = 0$. Since, in general, $\lambda_{eq} \geq 0$, the input bunch size is always larger than the corresponding equilibrium (matched) size, and the amount of mismatch is growing from head to tail as $\sqrt{1+\lambda_{eq}(\zeta)}$. Note that if, at injection, the system is initialized according to Eq. (22) it will remain in equilibrium, provided that the acceleration is adiabatic. At injection, and if $\lambda_i \ll 1$, the following approximate expressions hold, $\lambda_{eq} \simeq \lambda_i$, and $\langle x^2\rangle_{eq}(\zeta; z=0) \simeq (2/\gamma_i)^{1/2}(\varepsilon_{x,0}/k_p)[1-\lambda_i(\zeta)/2]$.

The initial slice-dependent mismatch causes the bunch moments on each slice to oscillate about the equilibrium values Eq. (22). In this model the mismatch of each slice is not damped because forces are linear. However, in the actual beam the mismatch will eventually be dissipated by phase-mixing due to the nonlinear component of the force. This, in addition to the slice-by-slice decoherence due to the slice-dependent betatron frequency, leads to the growth of the projected emittance from ion motion within a few betatron periods from injection. This process was investigated analytically in Ref. 19, where an expression for the saturated emittance as a function of beam and plasma parameters was provided.

The secular growth of the emittance can be evaluated from the equilibrium solution. In fact, we know from the simulations presented in Sec. II C that the secular growth is the same for untapered and tapered (equilibrium) bunches. By longitudinally averaging, according to Eq. (19), the equilibrium moments given in Eq. (22), we obtain the energy-dependent value of the projected emittance, that reads

$$\frac{\varepsilon_x}{\varepsilon_{x,0}} = \left[\overline{\left(\frac{1}{\sqrt{1+\lambda_{eq}}}\right)}\;\overline{\sqrt{1+\lambda_{eq}}}\right]^{1/2}. \quad (23)$$

For any given bunch energy, solution of Eq. (22a) provides $\langle x^2\rangle_{eq}$ and λ_{eq} along the bunch. The latter is used in Eq. (23) to compute the corresponding value of the projected emittance. Once the dependence of the projected emittance from the bunch energy is known, Eq. (18) can be used to determine the evolution of the emittance as a function of the propagation distance. We see that a growth of the projected emittance is always present whenever there is an energy-dependent, longitudinal variation of the betatron period. In fact, if λ_{eq} is slice-dependent, the right hand side of Eq. (23) is necessarily larger than one, and its magnitude increases as the chirp of the betatron wavenumber becomes larger, as is the case with ion motion. Hence, as was shown in the simulations presented in Sec. II C, the emittance growth is purely due to the differential evolution of the different witness bunch slices.

A simplified expression for the emittance growth valid in the limit $\lambda_{eq} \ll 1$ and at early times (i.e., when the equilibrium bunch is close to the input one) can be obtained by noticing that, according to Eq. (16), $\lambda_{eq} \sim 1/\langle x^2\rangle_{eq}$, and since $\langle x^2\rangle_{eq} \propto \gamma^{-1/2}$ we can explicitly factorize the dependence of λ_{eq} on the energy, while its $\zeta-$dependence is determined by the expression of λ at injection, namely

$$\lambda_{eq} \simeq \sqrt{\frac{\gamma}{\gamma_i}}\lambda_i. \quad (24)$$

By using this expression into Eq. (23), the projected emittance at early times reads

$$\frac{\varepsilon_x}{\varepsilon_{x,0}} \simeq 1 + \frac{1}{8}\frac{\gamma}{\gamma_i}\left(\overline{\lambda_i^2} - \overline{\lambda_i}^2\right) \simeq \frac{1}{8}\left(1+\frac{\gamma'}{\gamma_i}z\right)\left(\overline{\lambda_i^2} - \overline{\lambda_i}^2\right). \quad (25)$$

In Fig. 8 we compare the evolution of the projected emittance from PIC simulations (black line), to that obtained by numerically integrating Eq. (17) with the initial condition Eq. (20) (red line), and to the theoretical predictions Eq. (23) (blue line) and Eq. (25) (dotted cyan line, expression valid at early times) for a bunch with an injection energy of 50 MeV and different values of the initial emittance, namely $\varepsilon_{x,0} = 3$ μm, and $\varepsilon_{x,0} = 4$ μm. All the other bunch and plasma parameters are as in Sec. II. The (significantly) larger values of the emittance used here compared to the cases discussed in Sec. II and Sec. III were chosen so ion motion is not too severe during the early stages of the acceleration (in fact, at injection $\Lambda \simeq 0.1$ for $\varepsilon_{x,0} = 3$ μm, and $\Lambda \simeq 0.08$ for $\varepsilon_{x,0} = 4$), and so a comparison with theory is possible. Using the formalism developed here for the witness bunch parameters

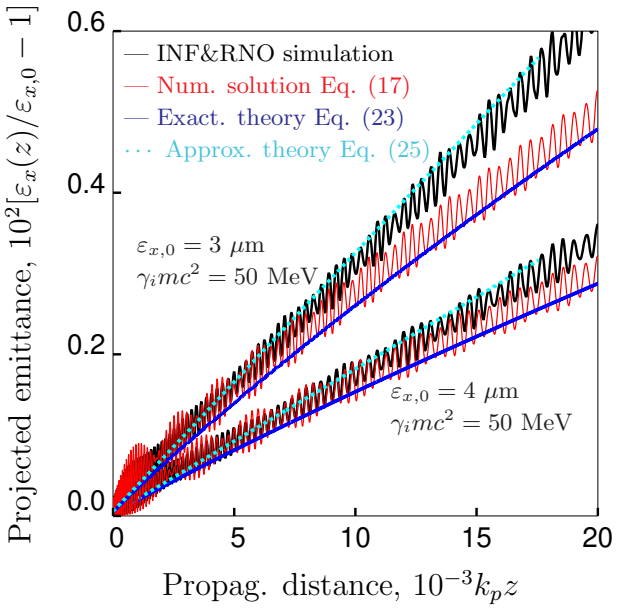

FIG. 8. Comparison of the evolution of the projected emittance from PIC simulations (black line), to that obtained by numerically integrating Eq. (17) with the initial condition Eq. (20) (red line), and to the theoretical predictions Eq. (23) (blue line) and Eq. (25) (dotted cyan line, expression valid at early times) for a bunch with an injection energy of 50 MeV and different values of the initial emittance, namely $\varepsilon_{x,0} = 3$ μm, and $\varepsilon_{x,0} = 4$ μm.

in Sec. II and Sec. III, requires an accurate expression for the ion-motion perturbed betatron wavenumber and its dependence on bunch energy valid when ion motion perturbation is severe.

We see that, at least for $k_p z \lesssim 12000$ in the case $\varepsilon_{x,0} = 4$ μm (~ 3.4 GeV energy gain), or $k_p z \lesssim 7000$ (~ 2 GeV energy gain) in the case $\varepsilon_{x,0} = 3$ μm, the emittance evolution obtained from the numerical integration of the moments model agrees with the one from the PIC simulation, confirming the validity of the former. The difference arising for longer propagation distances is due to the fact that, as a consequence of bunch compression during acceleration, ion motion grows and the assumption that background ion perturbation is small is no longer satisfied (i.e., $\Lambda \sim 1$). In this limit, the theory underestimates ion motion effects. We also note that, since at injection $\Lambda \ll 1$ (i.e., the injection energy is well below $\tilde{\gamma}_i mc^2$), the condition for adiabatic matching is well satisfied. Hence, the initial bunch mismatch is small and there is no emittance growth at injection. However, the secular growth of the emittance is present and it is in agreement with the theoretical prediction Eq. (23) (blue line), and Eq. (25) (cyan line) for early times.

V. CONCLUSIONS

We have presented and analyzed a plasma-based scheme to generate longitudinally shaped witness particle bunches that are equilibrium solutions in the presence of ion motion. In Ref. 25, the betatron frequency chirp resulting from ion-motion has been proposed as a possible way to suppress the hosing instability of a witness bunch with collider-relevant parameters accelerating in a PA stage in the blowout regime. The use of optimally tapered bunches can mitigate the residual ion-motion-induced emittance growth allowing for stable and high-quality acceleration of particle bunches, and, hence, enabling the use of plasma-based accelerators for high-energy physics applications.

The proposed scheme relies on an adiabatic matching procedure where a witness bunch with an initially untapered profile is injected in the PA stage with an energy low enough that ion motion effects are initially small. As the bunch accelerates it is adiabatically compressed, ion motion is triggered, and this results in the perturbation of the transverse wakefield. However, since changes due to acceleration are slow compared to betatron motion, the bunch readjusts itself during acceleration acquiring the desired taper, while maintaining every slice in a condition of equilibrium and, hence, the slice emittance is (quasi-)preserved in the process. However, as a consequence of the taper, the projected emittance displays a small growth that saturates at high energy.

The adiabatic matching process was studied analytically by means of a moments description for the bunch. A theory for the growth of the projected emittance, valid at early times and when ion motion is not too severe, was developed.

The method has been used to study the production of tapered beams in case of witness electron bunches with collider-relevant parameters (i.e., high charge, low emittance, low energy spread) and it was shown that for a sufficiently low injection energy of, e.g., ~ 50 MeV, much lower than the proposed 10s of GeV injection energy, only a moderate degradation of both the slice and the projected emittance is observed. Namely, projected emittance saturates after a $\sim 15\%$ growth, while the slice emittance acquires a head-to-tail taper of $\lesssim 10\%$. On the other hand, for an injection energy of 10 GeV, the projected emittance grows by more than $\sim 50\%$, and the slice emittance by more than $\sim 80\%$, after a few betatron periods. Emittance degradation is expected to be higher for an even higher injection energy. Low-injection energies favor plasma-based schemes for the production of witness bunches (e.g., two-color laser ionization[35,36], density-gradient injection[37–40], etc.).

This work did not consider the role of a plasma ramp at the entrance of the PA stage. However, we expect that a long (i.e., longer than the betatron period) plasma ramp, where the strength of the wakefield slowly increases as the bunch propagates through it, might be beneficial to the adiabatic matching procedure. Future studies will

address this subject.

Note that a plasma-based LC will require cascading several PA stages to reach the desired final energy. However, adiabatic matching is only required at the entrance of the first PA stage, where an untapered bunch is injected. Once the witness bunch reaches the tapered equilibrium profile it will remain matched as it is transported among the different stages.

Realization of a PA-based, TeV-class collider is a highly challenging task. Any strategy, like the adiabatic matching discussed here, which can help preserving the witness beam quality should be taken into consideration when designing such a device.

Even though the adiabatic matching method was proposed in the context of ion motion, it could be used to generate equilibrium bunch profiles in all the cases where the focusing force acting on the witness bunch is nonlinear, slice-dependent, and changes slowly with energy, provided that for a low enough energy a state exists where such forces are uniform along the bunch and the nonlinearity is small. Analysis of the method in other regimes will be a subject of future studies.

ACKNOWLEDGMENTS

This work was supported by the Director, Office of Science, Office of High Energy Physics, of the U.S. Department of Energy under Contract No. DE-AC02-05CH11231, and used the computational facilities at the National Energy Research Scientific Computing Center (NERSC).

The data that support the findings of this study are available from the corresponding author upon reasonable request.

[1] W. P. Leemans and E. Esarey, Phys. Today **62**, 44 (2009).
[2] C. B. Schroeder, E. Esarey, C. G. R. Geddes, C. Benedetti, and W. P. Leemans, Phys. Rev. ST Accel. Beams **13**, 101301 (2010).
[3] E. Adli, J. P. Delahaye, S. J. Gessner, M. J. Hogan, T. Raubenheimer, W. An, W. Mori, C. Joshi, and P. Muggli, in Proceedings of IPAC2013 (JACoW, 2013) p. TUPME020.
[4] K. Nakajima, A. Deng, X. Zhang, B. Shen, J. Liu, R. Li, Z. Xu, T. Ostermayr, S. Petrovics, C. Klier, K. Iqbal, H. Ruhl, and T. Tajima, Phys. Rev. ST Accel. Beams **14**, 091301 (2011).
[5] C. Joshi, S. Corde, and W. B. Mori, Phys. Plasmas **27**, 070602 (2020).
[6] E. Esarey, C. B. Schroeder, and W. P. Leemans, Rev. Mod. Phys. **81**, 1229 (2009).
[7] X. Wang, R. Zgadzaj, N. Fazel, Z. Li, S. A. Yi, X. Zhang, W. Henderson, Y.-Y. Chang, R. Korzekwa, H.-E. Tsai, C.-H. Pai, H. Quevedo, G. Dyer, E. Gaul, M. Martinez, A. C. Bernstein, T. Borger, M. Spinks, M. Donovan, V. Khudik, G. Shvets, T. Ditmire, and M. C. Downer, Nat. Commun. **4**, 1988 (2013).
[8] W. P. Leemans, A. J. Gonsalves, H.-S. Mao, K. Nakamura, C. Benedetti, C. B. Schroeder, Cs. Tóth, J. Daniels, D. E. Mittelberger, S. S. Bulanov, J.-L. Vay, C. G. R. Geddes, and E. Esarey, Phys. Rev. Lett. **113**, 245002 (2014).
[9] A. J. Gonsalves, K. Nakamura, J. Daniels, C. Benedetti, C. Pieronek, T. C. H. de Raadt, S. Steinke, J. H. Bin, S. S. Bulanov, J. van Tilborg, C. G. R. Geddes, C. B. Schroeder, Cs. Tóth, E. Esarey, K. Swanson, L. Fan-Chiang, G. Bagdasarov, N. Bobrova, V. Gasilov, G. Korn, P. Sasorov, and W. P. Leemans, Phys. Rev. Lett. **122**, 084801 (2019).
[10] I. Blumenfeld, C. E. Clayton, F.-J. Decker, M. J. Hogan, C. Huang, R. Ischebeck, R. Iverson, C. Joshi, T. Katsouleas, N. Kirby, W. Lu, K. A. Marsh, W. B. Mori, P. Muggli, E. Oz, R. H. Siemann, D. Walz, and M. Zhou, Nature **445**, 741 (2007).
[11] S. Corde, E. Adli, J. M. Allen, W. An, C. I. Clarke, C. E. Clayton, J. P. Delahaye, J. Frederico, S. Gessner, S. Z. Green, M. J. Hogan, C. Joshi, N. Lipkowitz, M. Litos, W. Lu, K. A. Marsh, W. B. Mori, M. Schmeltz, N. Vafaei-Najafabadi, D. Walz, V. Yakimenko, and G. Yocky, Nature **524**, 442 (2015).
[12] J. Ellis and I. Wilson, Nature **409**, 431 (2001).
[13] I. Hinchliffe and M. Battaglia, Phys. Today **57**, No. 9, 49 (2004).
[14] J. P. Delahaye, E. Adli, S. J. Gessner, M. J. Hogan, T. O. Raubenheimer, W. An, C. Joshi, W. B. Mori, in Proceedings of IPAC2014 (JACoW, 2014) p. THPRI013.
[15] V. Lebedev, A. Burov, and S. Nagaitsev, Phys. Rev. Accel. Beams 20, 121301 (2017).
[16] D. H. Whittum, W. M. Sharp, S. S. Yu, M. Lampe, and G. Joyce, Phys. Rev. Lett. 67, 991 (1991).
[17] Y. Y. Lau, Phys. Rev. Lett.63, **1141** (1989).
[18] J. B. Rosenzweig, A. M. Cook, A. Scott, M. C. Thompson, and R. B. Yoder, Phys. Rev. Lett. **95**, 195002 (2005).
[19] C. Benedetti, C. B. Schroeder, E. Esarey, and W. P. Leemans, Phys. Rev. Accel. Beams **20**, 111301 (2017).
[20] W. An, W. Lu, C. Huang, X. Xu, M. J. Hogan, C. Joshi, and W. B. Mori, Phys. Rev. Lett. **118**, 244801 (2017).
[21] V. E. Balakin, A. V. Novokhatsky, and V. P. Smirnov, in Proceedings, 12th International Conference on High-Energy Accelerators, HEACC 1983: Fermilab, Batavia (1984), pp. 119–120.
[22] J. Vieira, W. B. Mori, and P. Muggli, Phys. Rev. Lett. **112**, 205001 (2014).
[23] T. J. Mehrling, R. A. Fonseca, A. Martinez de la Ossa, and J. Vieira, Phys. Rev. Lett. **118**, 174801 (2017).
[24] R. Lehe, C. B. Schroeder, J.-L. Vay, E. Esarey, and W. P. Leemans, Phys. Rev. Lett. **119**, 244801 (2017).
[25] T. J. Mehrling, C. Benedetti, C. B. Schroeder, E. Esarey, and W. P. Leemans, Phys. Rev. Lett. **121**, 264802 (2018).
[26] R. Gholizadeh, T. Katsouleas, P. Muggli, C. Huang, and W. B. Mori, Phys. Rev. Lett. **104**, 155001 (2010).
[27] C. Benedetti, C. B. Schroeder, E. Esarey, C. G. R. Geddes, and W. P. Leemans, AIP Conference Proceedings **1299**, 250 (2010).
[28] C. Benedetti, C. B. Schroeder, C. G. R. Geddes, E. Esarey, and W. P. Leemans, Plasma Physics and Controlled Fusion **60** (2017).
[29] C. Benedetti, C. B. Schroeder, E. Esarey, C. G. R. Geddes, and W. P. Leemans, AIP Conference Proceedings **1812**, 050005 (2017).
[30] T. J. Mehrling, C. Benedetti, C. B. Schroeder, and J. Osterhoff, Plasma Phys. Control. Fusion **56**, 084012 (2014).
[31] T. J. Mehrling, C. Benedetti, C. B. Schroeder, and E. Esarey, A subgrid algorithm for the efficient modeling of plasma-based accelerators with ion motion using quasi-static particle-in-cell codes, in 2018 IEEE Advanced Accelerator-Concepts Workshop (AAC), Breckenridge, CO, USA(2019), https://doi.org/10.1109/AAC.2018.8659404.
[32] M. Tzoufras, W. Lu, F. S. Tsung, C. Huang, W. B. Mori, T. Katsouleas, J. Vieira, R. A. Fonseca, and L. O. Silva, Phys. Rev. Lett. **101**, 145002 (2008).
[33] D. L. Bruhwiler and D. A. Dimitrov, Phys. Plasmas **10**, 2022 (2003).
[34] M. Bell and J. S. Bell, Part. Accel. **24**, 1 (1988).
[35] L.-L. Yu, E. Esarey, C. B. Schroeder, J.-L. Vay, C. Benedetti, C. G. R. Geddes, M. Chen, and W. P. Leemans, Phys. Rev. Lett. **112**, 125001 (2014).
[36] P. Tomassini, D. Terzani, L. Labate, G. Toci, A. Chance, P. A. P. Nghiem, and L. A. Gizzi, Phys. Rev. Accel. Beams **22**, 111302 (2019).
[37] S. Bulanov, N. Naumova, F. Pegoraro, and J. Sakai, Phys. Rev. E **58**, R5257 (1998).

[38] C. G. R. Geddes, K. Nakamura, G. R. Plateau, Cs. Tóth, E. Cormier-Michel, E. Esarey, C. B. Schroeder, J. R. Cary, and W. P. Leemans, Phys. Rev. Lett. **100**, 215004 (2008).

[39] A. J. Gonsalves, K. Nakamura, C. Lin, D. Panasenko, S. Shiraishi, T. Sokollik, C. Benedetti, C. B. Schroeder, C. G. R. Geddes, J. van Tilborg, J. Osterhoff, E. Esarey, C. Tóth, and W. P. Leemans, Nature Phys. **7**, 862 (2011).

[40] X. L. Xu, F. Li, W. An, T. N. Dalichaouch, P. Yu, W. Lu, C. Joshi, and W. B. Mori, Phys. Rev. Accel. Beams **20**, 111303 (2017).